



1 **Comparing soil moisture anomalies from multiple independent sources over**  
2 **different regions across the globe**

3

4 Carmelo Cammalleri, Jürgen V. Vogt, Bernard Bisselink, Ad de Roo

5 European Commission, Joint Research Centre (JRC), Ispra, Italy.

6

7 *Correspondence to:* C. Cammalleri, European Commission - Joint Research Centre, via E. Fermi 2749,  
8 I-21027 Ispra (VA), Italy. Bldg. 100, Room 1208, TP 122. Phone: +39 (0)332.78.9869, e-mail:  
9 carmelo.cammalleri@ec.europa.eu.

10

11 **Abstract:** Agricultural drought events can affect large regions across the World, implying the urge for a  
12 suitable global tool for an accurate monitoring of this phenomenon. Soil moisture anomalies are  
13 considered a good metric to capture the occurrence of agricultural drought events, and they have  
14 become an important component of several operational drought monitoring systems. In the framework  
15 of the JRC Global Drought Observatory (GDO, <http://edo.jrc.ec.europa.eu/gdo/>) the suitability of  
16 modelled and/or satellite-derived proxy of soil moisture anomalies was investigated. In this study, three  
17 datasets have been evaluated as possible proxies of root zone soil moisture anomalies: (1) soil moisture  
18 from the Lisflood distributed hydrological model (LIS), (2) remotely sensed land surface temperature  
19 data from the MODIS satellite (LST), and (3) the combined passive/active microwave skin soil moisture  
20 dataset developed by ESA (CCI). Due to the independency of these three datasets, the Triple  
21 Collocation (TC) technique has been applied, aiming at quantifying the likely error associated to each



22 dataset in comparison to the unknown true status of the system. TC analysis was performed on five  
23 macro-regions (namely North America, Europe, India, Southern Africa and Australia) detected as  
24 suitable for the experiment, providing insight into the mutual relationship between these datasets as well  
25 as assessment of the accuracy of each method. A clear outcome of the TC analysis is the good  
26 performance of remote sensing datasets, especially CCI, over dry regions such as Australia and  
27 Southern Africa, whereas the outputs of LIS seem to be more reliable over areas that are well monitored  
28 through meteorological ground station networks, such as North America and Europe. In a global  
29 drought monitoring system, these results can be used to design an ensemble system that exploits the  
30 advantages of each dataset.

31

## 32 **1. Introduction**

33

34 Drought is a recurring natural extreme, triggered by lower than normal rainfall, often exacerbated  
35 by a strong evaporative demand due to high temperatures and strong winds. Drought events may occur  
36 in all climates and in most parts of the world, since drought is defined as a temporary deviation from the  
37 local normal condition. Due to the usually wide extension of the interested area, drought affects millions  
38 of people across the Globe each year (Wilhite, 2000).

39 On the basis of the economic and natural sectors impacted by this phenomenon, a drought event is  
40 usually classified in meteorological, agricultural and hydrological drought, depending on the persistence  
41 of the water deficit within the hydrological cycle. Of particular interest for this study are the agricultural



42 (or ecosystem) drought events, defined as prolonged periods with drier than usual soils that negatively  
43 affect vegetation growth and crop production, and, as a consequence, human welfare (Dai, 2011).

44 Soil moisture is commonly seen as one of the most suitable variables to monitor and quantify the  
45 impact of water shortage on vegetated lands due to its effects on the terrestrial biosphere and the  
46 feedback into the atmospheric system, as highlighted by the inclusion of soil moisture anomalies in  
47 numerous drought monitoring systems at regional to continental scales (i.e., European Drought  
48 Observatory, United States Drought Monitor, African Flood and Drought Monitor, among others).

49 Soil moisture monitoring over large areas is usually obtained through either distributed  
50 hydrological models or land-surface schemes of climate models (Crow et al., 2012; Sheffield et al.,  
51 2004), as well as by thermal or passive/active microwave remote sensing-derived quantities (see e.g.,  
52 Anderson et al., 2007; Houborg et al., 2012; Mo et al., 2010). In the context of a global drought  
53 monitoring system, remote sensing-based approaches have the advantage of an intrinsic worldwide  
54 coverage, but the drawbacks, in the case of microwave sensors, of exploring only the first few  
55 centimeters of soil and a decreasing sensitivity with the increase of vegetation coverage (Jackson,  
56 2006). In the case of thermal data, the lack of coverage during cloudy conditions and the nontrivial  
57 connection between thermal and soil moisture signals (Price, 1980) are other limitations. On the  
58 contrary, diagnostic models allow for a continuous monitoring of soil moisture at the desired soil  
59 depths, but the accuracy of the data is constrained by uncertainties in the parameterization of soil  
60 hydrological characteristics, as well as by the actual availability of near-real time reliable  
61 meteorological forcing data. Generally, the use of in-situ observations for large area monitoring is



62 limited, mainly due to the lack of long records, the sparseness of recording stations and the high spatial  
63 heterogeneity of soil moisture fields.

64 It follows that both satellite measurements and model predictions are subject to errors and  
65 uncertainties that need to be accounted for in their interpretation and application (Gruber et al., 2016).  
66 This also suggests that a monitoring system based on a single model is rarely capable to provide global  
67 reliable estimates, and a combination of different data sources is desirable in order to minimize the  
68 errors in the detection of drought events. Recently, Cammalleri et al. (2015) demonstrated the value of  
69 an ensemble of modelled soil moisture anomalies for drought monitoring over Europe, similarly to the  
70 findings of the U.S. National Land Data Assimilation System (NLDAS) (Dirmeyer et al., 2006).  
71 However, a key point in combining different modelled data is the need to estimate the affinity and  
72 divergence between the models across the modelling domain.

73 In the most recent years, the Triple Collocation (TC) technique (Stoffelen, 1998) has been  
74 established as a practical approach to evaluate the unknown error variance (with respect to the truth) of  
75 three mutually independent measurement systems without knowing the “true” status of the system  
76 (Yilmaz and Crow, 2014). This technique has been widely applied in hydrology to estimate errors in  
77 soil moisture, as well as to evaluate precipitation and vegetation property indicators (Dorigo et al.,  
78 2010; McColl et al., 2014). One key requirement in TC is the existence of linearity between the three  
79 estimates and the truth, which can fail in the case of strongly seasonal geophysical variables such as soil  
80 moisture (Su et al., 2014). Luckily, drought monitoring systems are usually based on soil moisture  
81 anomalies rather than actual values, hence providing a partial remedy to this problem and making soil  
82 moisture anomalies directly suitable for this methodology (Miralles et al., 2010).



83 In the frame of the operational monitoring of agriculture and ecosystem drought conditions in the  
84 Global Drought Observatory (GDO, <http://edo.jrc.ec.europa.eu/gdo/>), developed by the Joint Research  
85 Centre (JRC) of the European Commission, the soil moisture outputs of the Lisflood hydrological  
86 model and the land surface temperature (LST) anomalies derived from the Moderate-Resolution  
87 Imaging Spectroradiometer (MODIS) onboard the Terra satellite have been detected as suitable datasets  
88 for a near-real time monitoring. In particular, Cammalleri and Vogt (2016) have highlighted how LST  
89 anomalies represent the best proxy of soil moisture variations across different climates in Europe when  
90 compared to other LST-derived quantities.

91 As a third dataset for the TC analysis, the combined active/passive microwave soil moisture  
92 dataset produced by the European Space Agency (ESA) in the context of the Climate Change Initiative  
93 (CCI) is used; even if this dataset is not updated in near-real time, it represents a valuable reference  
94 dataset for a global consistent time-series of microwave-based soil moisture maps. The use of three  
95 independent sources of data (hydrological model, thermal and microwave remote sensing) helps  
96 ensuring to fulfill a key hypothesis of TC, which is the independency between the errors of the three  
97 models.

98 The overall goal of this study is twofold. First, the agreement between the monthly anomalies of  
99 the three models is evaluated, in order to identify the macro-areas where a reliable monitoring of soil  
100 moisture extreme conditions can be performed according to the available datasets. Second, the TC  
101 analysis is performed over those macro-areas to quantify the spatial distribution of the expected random  
102 errors for each model compared to the unknown true status in order to develop a suitable combination  
103 procedure for a near-real time detection of the occurrence of ecosystem drought events. Both goals will



104 contribute to the development of a robust agricultural drought monitoring index within the GDO  
105 system.

106

## 107 2. Methods

108

109 Drought events are commonly defined as prolonged periods during which a given drought  
110 indicator significantly deviates from the usual condition for the specific site and period (e.g., soil  
111 moisture content is lower than the climatology). Following this definition, this study will focus on  
112 standardized z-score values in order to make directly comparable the different datasets (i.e., minimizing  
113 the differences related to seasonality, soil depth, etc.). Specifically, monthly z-score values, or  
114 anomalies, are evaluated as:

$$115 \quad Z_{x,i,k} = \frac{x_{i,k} - \mu_{x,i}}{\sigma_{x,i}} \quad (1)$$

116 where  $x_{i,k}$  is the monthly average variable for the  $i$ -th month at the  $k$ -th year,  $\mu_{x,i}$  and  $\sigma_{x,i}$  are the long-  
117 term average and standard deviation of the variable  $x$  for the  $i$ -th month, respectively. The baseline  
118 period adopted to compute the reference  $\mu$  and  $\sigma$  twelve monthly values should be of 15-30 years in  
119 order to ensure a stable benchmark. The three datasets used here, as described in the next section, are  
120 the root zone soil moisture data from the Lisflood model ( $x = LIS$ ), the ESA skin soil moisture  
121 microwave combined product ( $x = CCI$ ) and the thermal remote sensing derived land surface  
122 temperature ( $x = LST$ ); in the case of LST data, the sign of the anomalies is reversed due to the expected  
123 inverse relationship between soil moisture and LST.



124 The time-series of anomalies computed according to Eq. (1) are characterized by a null average  
125 and a unitary standard deviation, making a direct comparison of the different datasets simpler;  
126 additionally, in this particular case the Pearson correlation coefficient,  $R$ , represents not only a measure  
127 of the linear dependency of the two random quantities but also the slope of the linear relationship and a  
128 proxy of the difference and biases of the two datasets. In this respect,  $R$  can be seen as a good synthetic  
129 descriptor of the relationship between two standardized z-score datasets. The statistical significance of  
130 the existence of a positive correlation can be evaluated by means of the t-student test (2 sided) by  
131 computing the  $R$  value corresponding to a significance level  $p = 0.05$ .

132 Analysis of the correlation among the datasets is interesting in the framework of the triple  
133 collocation (TC) technique and its basic hypotheses. In TC, a first key hypothesis is the existence of  
134 linearity between the ‘true’ status of the system and the three models; this is formally expressed as:

$$135 \quad z_x = \alpha_x + \beta_x z_\Theta + \varepsilon_x \quad (2)$$

136 where  $z_\Theta$  is the unknown true dataset of soil moisture anomalies,  $\alpha_x$  and  $\beta_x$  are the systematic slope and  
137 bias parameters for the dataset  $x$  with respect to the truth, and  $\varepsilon_x$  is the additive zero-mean random noise.  
138 It follows that the absence of a statistical significant linear relation between all three models openly  
139 violates this hypothesis.

140 Other key underlying hypotheses of TC are the stationarity of both signals and errors, the  
141 independency between the errors and the signal (error orthogonality) and the independence between the  
142 errors of the three datasets (zero-cross correlation) (Gruber et al., 2016). Under these assumptions,  
143 Stoffelen (1998) proposed a formulation to estimate each model error variance,  $\sigma_{\varepsilon_x}^2$ , based on a  
144 combination of the covariance between the datasets. In this approach, known as the covariance notation



145 (Gruber et al., 2016), the error variance values are computed without a common (arbitrary) reference  
146 dataset as:

$$\begin{aligned} \sigma_{\varepsilon_1}^2 &= \sigma_1^2 - \frac{\sigma_{12}\sigma_{13}}{\sigma_{23}} \\ \sigma_{\varepsilon_2}^2 &= \sigma_2^2 - \frac{\sigma_{21}\sigma_{23}}{\sigma_{13}} \\ \sigma_{\varepsilon_3}^2 &= \sigma_3^2 - \frac{\sigma_{31}\sigma_{32}}{\sigma_{12}} \end{aligned} \quad (3)$$

148 where, for the sake of simplicity, LIS, LST and CCI were renamed 1, 2, 3, respectively. The first term  
149 on the right side of Eqs. (3) represents the single model data variance, whereas the second term  
150 represents the so-called sensitivity of the model to variations in the true status, which is a function of the  
151 covariance terms between the three models. The advantage of this formulation is to directly estimate the  
152 unscaled error variances, which can (eventually) be scaled to a common data space, if needed.

153 Different performance metrics can be derived from the covariance notation, including relative  
154 error variance metrics such as the fractional root-mean-squared-error (fRMSE, Draper et al., 2013) and  
155 the correlation coefficient of each model with the underlying true signal (McColl et al., 2014).  
156 However, these metrics can be derived from each other by means of simple relationships (see Gruber et  
157 al., 2016) and they are analogous to the absolute error values in the case of z-score values that have  
158 known unitary dataset variance.

159

### 160 **3. Data and Materials**

161

#### 162 ***3.1 Lisflood model soil moisture***

163





164 Root zone soil moisture dynamics are simulated by means of the Lisflood model (de Roo et al.,  
165 2000), a GIS-based distributed hydrological rainfall-runoff-routing model designed to reproduce the  
166 main hydrological processes that occur in large and trans-national European river catchments. The  
167 model simulates all the main hydrological processes occurring in the land-atmosphere system, including  
168 infiltration, actual evapotranspiration, soil water redistribution in three sub-layers (surface, root zone  
169 and sub-soil), surface runoff routing to channel, and groundwater storage and transport (Burek et al.,  
170 2013).

171 Static maps used by the model are related to topography (i.e., digital elevation model, local drain  
172 direction, slope gradient, elevation range), land use (i.e., land use classes, forest fraction, fraction of  
173 urban area), soil (i.e., soil texture classes, soil depth), and channel geometry (i.e., channel gradient,  
174 Manning's roughness, bankfull channel depth, channel length, bottom width and side slope). The soil-  
175 related quantities are obtained from the ISRIC 1-km SoilGrids database (Hengl et al., 2014), whereas  
176 topography data are obtained from the Hydrosheds database (Lehner et al., 2008).

177 Daily meteorological forcing maps are derived from the European Centre for Medium-range  
178 Weather Forecasts (ECMWF) data as spatially resampled and harmonized by the JRC Monitoring  
179 Agricultural ResourceS (MARS) group. The dataset includes daily average air temperature, potential  
180 evapotranspiration (for soil, water and reference surfaces) and total rainfall at 0.25 degree spatial  
181 resolution, which were resampled on the model grid using the nearest neighbors algorithm.

182 The model run used in this study includes daily maps at 0.1 degree resolution between 1989 and  
183 2015; the grid domain of this dataset is used as reference for the other two, whereas the baseline for the  
184 anomalies computation is defined by the period 2001-2015 in order to match the LST data availability.



185 Monthly data to be used in Eq. (1) are computed as a simple average of all the data available for each  
186 month, given that no gaps can be found in this dataset due to its continuous nature as hydrological  
187 model. However, some areas were masked out due to the minimum or null temporal dynamic of soil  
188 moisture, such as Greenland and the Sahara desert.

189

### 190 *3.2 Land Surface Temperature dataset*

191

192 The use of the land surface temperature (LST) anomalies as a proxy of soil moisture anomalies is  
193 based on the well-known role of LST in the surface energy budget as a control factor for the partitioning  
194 between latent and sensible heat fluxes. In recent years, the existence of a connection between soil  
195 moisture and LST has been analyzed, mainly through the thermal inertia and the triangle methods (e.g.,  
196 Carlson 2007; Verstraeten et al., 2006), as well as a direct proxy (see e.g., Park et al., 2014; Srivastava  
197 et al., 2016). In a study over the pan-European domain, Cammalleri and Vogt (2016) have demonstrated  
198 the good agreement between monthly LST and soil moisture z-score values during summer time, where  
199 LST outperforms other LST-based indicators such as the day-night difference and the surface-air  
200 gradient.

201 Following these findings, this study adopts the dataset collected by the Moderate-Resolution  
202 Imaging Spectroradiometer (MODIS) sensor on board of the Terra satellite  
203 (<http://terra.nasa.gov/about/terra-instruments/modis>) as a source of monthly-scale long records of LST  
204 maps. In particular, the MOD11C3 Monthly CMG (Climate Modelling Grid) LST product is used in  
205 this study, which is constituted by monthly composited and averaged temperature and emissivity maps



206 at a spatial resolution of 0.05 degrees over a regular latitude/longitude grid; data for the period 2001–  
207 2015 are used, as the only fully completed years at the time of the analysis.

208 This monthly composite product is obtained as an average of the clear-sky data in the MOD11C1  
209 products on the calendar days of the specific month, which are derived after a re-projecting and a re-  
210 sampling of the MOD11B1 product. Details on the algorithms used to obtain the daily MOD11B1 maps  
211 can be found in Wan et al. (2002); in summary, a double screening procedure is applied, based on: i) the  
212 difference between the two independent LST estimates of the day/night algorithm (Wan and Li, 1997)  
213 and the generalized split-window algorithm (Wan and Dozier, 1996), and ii) the histogram of the  
214 difference between daytime and nighttime LSTs.

215 LST monthly maps were spatially co-registered to the Lisflood 0.1 degree regular  
216 latitude/longitude grid by means of a simple average of the values within each cell, and anomaly maps  
217 were computed according to Eq. (1) by using only the data for which  $LST > 1\text{ }^{\circ}\text{C}$ ; this threshold value  
218 (commonly used in snowmelt and snow/rainfall discrimination procedures; WMO, 1986) allows  
219 removing the data that are likely affected by snow/frost from the analysis.

220

### 221 ***3.3 Microwave combined dataset***

222

223 The ESA Climate Change Initiative (CCI) aims at developing a multi-satellite soil moisture  
224 dataset by combining data collected in both past and present by passive and active microwave  
225 instruments (Dorigo et al., 2016). The current version of the dataset combines data from nine different



226 sensors (SMMR, ERS-1/2, TMI, SSM/I, AMSR-E, ASCAT, WindSat, AMSR2 and SMOS) between  
227 1978 and 2015.

228 Satellite-based microwave estimates of soil moisture are usually related to the first few  
229 centimeters of soil column (i.e., skin layer), which is quite closely related to the soil moisture content in  
230 the root zone (Paulik et al., 2014), except for very dry conditions. Additionally, numerous validations  
231 against land surface models have highlighted good performance across the globe, with notable  
232 exceptions over densely vegetated areas (e.g., Loew et al., 2013).

233 The algorithm adopted to merge the different data sources is the one developed by Liu et al.  
234 (2012), which is a three-step procedure that: i) merges the original passive microwave products, ii)  
235 merges the original active microwave products, and iii) blends the two merged products into a single  
236 final dataset. The merging procedure of passive datasets includes pixel-scale separation between  
237 seasonality and anomalies, rescaling of the data based on the piece-wise cumulative distribution  
238 function (CDF) and merging of the dataset using a common reference seasonality. For the active  
239 microwave instruments, the CDFs are directly used to rescale the data under the assumption that active  
240 datasets have an identical dynamic range, this mainly due to the limited overlap between datasets. The  
241 final blending of the two merged datasets is obtained by adopting a common resolution of  
242 approximately 25 km and daily frequency, as well as by using the GLDAS-1-Noah model  
243 (<ftp://agdisc.gsfc.nasa.gov/data/s4pa/>) as a reference dataset for the CDF matching.

244 In this study, the daily blended dataset is spatially resampled to a 0.1 degree regular  
245 latitude/longitude grid (the same used in Lisflood simulations) by means of the nearest neighbor  
246 algorithm, and successively aggregated to monthly time scale by simply averaging the data (only if at



247 least 8 daily values were available in the specific month). Monthly average maps were converted into z-  
248 score maps by using the baseline period 2001-2015 (the timeframe available for the LST dataset).

249

#### 250 4. Results and Discussion

251

252 Considering the assumption of linearity between each one of the models and the unknown true  
253 status of the system in TC, a preliminary analysis on the linear correlation between the three models has  
254 been performed in order to detect the macro-areas where the TC procedure can be applied without  
255 violating this basic hypothesis. The correlation analysis was performed by using only the monthly data  
256 that were available for all three models, and by defining a minimum correlation threshold ( $R_{0.05}$ ) that  
257 ensures a statistical significance of the linear relationship on the basis of the t-student test (at  $p = 0.05$ ).

258 The map in Fig. 1 reports in grey the areas where all three models are significantly linearly  
259 correlated according to the described criteria, representing the areas where the first basic hypothesis of  
260 the TC is not clearly violated. It is worth to point out that some areas are excluded from the analysis by  
261 the lack of data in LIS (low temporal variability, as over Greenland and the Sahara desert), LST (due to  
262 the minimum temperature threshold or low temporal variability) or CCI (densely vegetated areas, such  
263 as Amazon forest and the Congo basin). These results suggest to focus the successive detailed analysis  
264 on five macro-regions (demarcated by the boxes in Fig. 1) that have consistent positive correlation values  
265 for all the three models; these areas are named, from now on, as: 1) NA (including the contiguous U.S.



266 and Mexico), 2) EU (Southern and Central Europe), 3) SA (Southern countries of the African continent  
267 and Madagascar), 4) IN (Indian subcontinent), and 5) AU (Australia)\*.

268 The correlation coefficient maps over those regions, obtained by inter-comparing the three  
269 models, are reported in Figs. 2 to 4, where the cells in red and yellow are the ones with negative or not-  
270 significant correlation, respectively, whereas the blue scale represents the cells with increasing  
271 significant linear correlation (from light to dark tones). The comparison between LIS and LST (Fig. 2)  
272 shows an overall good agreement between the two datasets, with only minor areas characterized by  
273 negative/not-significant correlation values; notably, low correlation can be observed over the Great  
274 Lakes and Rocky mountain areas in the U.S., over the Alps in Europe, North Angola and Western  
275 Himalaya. Similar results can be observed in Fig. 3, where LIS and CCI datasets are compared; this  
276 comparison shows an increasing number of negative values in Western U.S., the Alps, and Southern  
277 Turkey, but overall high correlation values across most of the five regions. Finally, the comparison  
278 between LST and CCI reported in Fig. 4 shows an increase of areas with low/not-significant correlation  
279 in Eastern and Western U.S. and both North- and South-Eastern Europe and the Alps, whereas a high  
280 correlation can be observed all over the other regions.

281 On average, the data in Table 1 summarize the results obtained for all the regions together, as well  
282 as for each region independently, showing how CCI and LST are the two datasets best correlated to  
283 each other overall, even if this result is mainly driven by the results over AU, SA and IN macro-areas.  
284 The data of the LIS model are similarly correlated to the ones of LST and CCI, with a more uniform  
285 distribution of the results across the various sub-regions. Another outcome of this analysis is that the

---

\* Consider the countries and boundaries reported here only as indicative of the interested areas, and they may not in any circumstances be regarded as stating an official position of the European Commission.



286 area with the lowest average correlation between the three models is EU, probably due to the high  
287 heterogeneity of this region at the 0.1 degree spatial scale.

288 Overall, the use of LST as proxy of soil moisture anomalies seems based on a reliable assumption,  
289 since there is a clear consistency of LST anomalies with the other two datasets. This consideration  
290 allows applying the TC analysis to the LST dataset as well, whereas most of the studies in the literature  
291 focus on land modelled and microwave soil moisture datasets (i.e., Dorigo et al., 2010; Gruber et al.,  
292 2016; Su et al., 2014) with only few notable exceptions including thermal data (e.g., Hain et al., 2011).

293 The outputs of the correlation analysis were used to detect the cells suitable for the TC technique;  
294 since a key hypothesis of the technique is the existence of a linear relation between each model and the  
295 (unknown) truth, a necessary condition (even if not sufficient) is the existence of linear relationships  
296 among the three models. As outcome of the correlation analysis, around 10% of the five macro-areas  
297 were removed from the TC analysis due to the absence of this basic condition.

298 The maps in Figs. 5 to 7 show the main outcome of the TC analysis, which is the spatial  
299 distribution of the error variance for each model, as detailed by Eqs. (3). The blank areas in those maps  
300 correspond to the cells where no significant linear correlation was observed between all three models.  
301 The results for LIS (Fig. 5) show how the highest errors are observed over the Western U.S., Northern  
302 Cape in South Africa and Western/Southern Australia, whereas low errors are observed over the Eastern  
303 U.S. On the opposite, the LST dataset displays the highest errors over the latter area (Fig. 6), whereas  
304 the lowest errors are observed over Queensland in Australia, Eastern Cape in South Africa and Lesotho.  
305 The maps in Fig. 7 show that the CCI dataset has consistent patterns of low error variance values over  
306 most of Australia, Western India and Central U.S.



307 Overall, on one hand, it seems evident how CCI tends to outperform the other two methods over  
308 dry areas such as Australia and South Africa, but on the other hand, a region like the U.S. is almost  
309 equally subdivided among the three models, where LIS performs better in the East, LST in the West and  
310 CCI in the center. Differences among models can be partially explained by the differences in the soil  
311 layer monitored by each dataset, i.e., microwave system capturing skin soil moisture whereas Lisflood  
312 models the full root zone; indeed, even if the use of monthly anomalies allows minimizing some of the  
313 discrepancies, skin soil moisture remains more reliable for dry/bare areas (Das et al., 2015).

314 These findings are summarized in the data reported in Table 2, where the average error variance  
315 for each model and macro-area is reported aside its spatial standard deviation. The data in Table 2  
316 confirm that CCI has an overall better performance (lower errors) than LIS and LST, which perform  
317 quite closely, mainly thanks to the very low error variance observed over Australia and, to a minor  
318 extend, Southern Africa. The LIS model shows to perform better over NA and EU regions, likely due to  
319 the better meteorological forcing datasets available over those regions compared to the other macro-  
320 areas (due to denser ground networks). The LST dataset seems to perform moderately well over all five  
321 macro-regions, with the only notable exception of EU; however, it rarely outperforms the other two  
322 datasets, constituting a “second-best” option in most of the cases. It is also worth to point out that the  
323 CCI dataset is often masked-out over those regions where the error of microwave techniques are likely  
324 high, whereas the data of the other two datasets are mostly produced globally; hence, a possible  
325 explanation of the better performance of CCI compared to LIS and LST may be linked to this  
326 preliminary screening of the data.





327 The outcome that LIS slightly outperforms the other two datasets over NA is in agreement with  
328 the results reported by Hain et al. (2011), where the Noah land-surface model slightly outperforms (on  
329 average) the microwave and thermal datasets over Contiguous U.S. However, it should be pointed out  
330 how the spatial distribution of the error estimates for LIS differs from the ones reported for Noah, likely  
331 due to the differences in both meteorological forcing and modelling approaches. Similarly, Pierdicca et  
332 al. (2015) shows smaller average errors over Europe for the ERA-LAND modelled datasets compared to  
333 two microwave-based datasets, similarly to the results obtained in this study. Both these results seem to  
334 suggest that land modelling approaches are more reliable, on average, over these regions, likely due to  
335 the reliability of meteorological forcing and model parameterizations, even if there can be significant  
336 differences among the performances of different land models.

337 Over AU sub-region, the spatial distribution of the errors in CCI are quite in agreement with the  
338 results reported in Su et al. (2014) for two microwave datasets, with larger errors along the South-East  
339 Australian coast. This result supports the assumption that microwave data are more reliable over dry  
340 bare soil areas, which is further highlighted by the results obtained in SA and IN sub-regions. The  
341 subdivision of the NA domain in three main regions is similar to the one observed by Gruber et al.  
342 (2016) in comparing ASCAT and AMSR-E microwave datasets, suggesting key differences in the soil  
343 moisture behavior over these three sub-regions. Overall, the spatial patterns of microwave and land  
344 model errors show similarities with the ones observed by Dorigo et al. (2010), even if no thermal data  
345 were included in their analysis.

346 The error variance values can also be interpreted as the correlation coefficient of each dataset with  
347 the underlying true signal, following the definition of McColl et al. (2014). In fact, for the special case



348 of anomalies with unitary variance ( $\sigma_x^2 = 1$ ), the TC-derived  $R_x$  of each dataset is simply equal to  
349  $\sqrt{1 - \sigma_{\varepsilon_x}^2}$ , which ranges on average over all five regions (not shown) between 0.91 (for CCI in AU) to  
350 0.66 (for LST over EU); these values show a good capability of the models to capture, on average,  
351 temporal variations in soil moisture anomalies.

352 In order to provide a simple synthetic representation of the likely best model for each area, the  
353 map in Fig. 8 depicts for each cell the dataset with the lowest error variance by associating different  
354 colors to the three models (red for LIS, blue for LST and green for CCI). Even if this approach is rather  
355 simplistic, as it cannot account for two models performing really close over some areas, the major  
356 relevant features, like the predominance of the CCI model over Australia, are made evident by these  
357 maps.

358 The maps in Fig. 8 confirm CCI as the dataset with the lowest error variance values over most of  
359 AU, SA and IN, whereas the three models almost equally split the other two macro-areas; this is even  
360 more evident in the data reported in Table 3, where the percentage of sub-areas where each model is the  
361 best is reported. These data confirm the good performance of CCI over AU, SA and IN macro-regions,  
362 whereas the NA territory is almost equally divided among the three datasets and LIS outperforms both  
363 LST and CCI over 50% of EU domain. In the latter, the areas where the LIS dataset outperforms the  
364 other two datasets partially resemble the results obtained by Pierdicca et al. (2011) for the ERA-LAND  
365 model; however, the present study includes also remote sensing thermal data and not only microwave-  
366 derived datasets. Overall, the CCI dataset outperforms the other two datasets in about 50% of cells, with  
367 the remaining almost equally split between LIS and LST.

368



## 369 5. Summary and Conclusions

370

371 Three datasets have been compared as proxy of the unknown true status of soil moisture  
372 anomalies in the context of the global drought monitoring system under development by the JRC of the  
373 European Commission. Key assumption of the study is the inability of a single dataset to accurately  
374 capture the soil moisture dynamic over the large range of variability of conditions that can be observed  
375 at continental to global scale.

376 The inter-comparison between the three datasets, namely the outputs of the Lisflood hydrological  
377 model (LIS), the MODIS-based land surface temperature (LST) and the combined active/passive  
378 satellite microwave (CCI) data, confirms inconsistencies between the three datasets over some areas, as  
379 well as the difficulties in comparing the three datasets over certain areas (e.g., Sahara desert, Amazon  
380 rainforest) due to the lack of coverage from one or more datasets. Focusing the analysis only on the  
381 areas where the three models are substantially in agreement (following a linear regression analysis), five  
382 macro-regions were detected as suitable for further investigations according to the Triple Collocation  
383 (TC) technique. This analysis allows quantifying the likely random error associated with each model  
384 (with regard to the true status) even in absence of an observation of the “truth”, under the hypothesis  
385 that certain criteria are met.

386 The main outcome of the TC analysis further confirms the need of a multi-source approach for a  
387 reliable assessment of soil moisture anomalies over those five regions, given that no model outperforms  
388 the others (in terms of expected error variance) for the entire study domain. Emblematic are the results  
389 over North America, where each model outperforms the others in one sub-region, like the LIS approach



390 in Eastern U.S., LST in the South-Western domain and CCI in Central U.S. Overall, remote sensing  
391 datasets seem to perform better over dry areas and sparsely monitored areas (e.g., Australia and  
392 Southern Africa), whereas the LIS dataset seems more reliable over NA and EU where dense networks  
393 of meteorological ground stations are deployed.

394 It has been highlighted how some differences among models can also be related to the soil layer  
395 monitored by each dataset, i.e., the microwave system capturing skin soil moisture whereas Lisflood  
396 models the full root zone; indeed, even if the use of monthly anomalies allows minimizing some of the  
397 discrepancies, our results confirm that skin soil moisture remains more reliable for dry/bare areas (Das  
398 et al., 2015), whereas hydrological models are more suited for agricultural regions. Some analogies  
399 between the obtained results and the ones already available in the literature have been found, but the  
400 inclusion of thermal data into the analysis enlarges the understanding of the mutual relationship  
401 between the different datasets.

402 The results of this study represent a robust starting point for the development of a global drought  
403 monitoring system based on such anomaly datasets, which can exploit the main findings of the TC  
404 analysis in order to develop a suitable ensemble product over the investigated regions. Further analyses  
405 are required to be able to extend the test to the areas currently not included in this study, especially the  
406 ones where the three datasets are available but provide inconsistent or contrasting results.

407



## 408 **References**

409

410 Anderson, M.C., Norman, J.M., Mecikalski, J.R., Otkin, J.P., Kustas, W.P., 2007. A climatological  
411 study of evapotranspiration and moisture stress across the continental U.S. based on thermal  
412 remote sensing: II. Surface moisture climatology. *J. Geophys. Res.* 112, D11112,  
413 doi:10.1029/2006JD007507.

414 Burek, P., van der Knijff, J.M., de Roo, A., 2013. LISFLOOD: Distributed Water Balance and Flood  
415 Simulation Model. JRC Scientific and Technical Reports, EUR 26162 EN, 142 pp.  
416 doi:10.2788/24719.

417 Cammalleri, C., Vogt, J.V., 2016. On the role of Land Surface Temperature as proxy of soil moisture  
418 status for drought monitoring in Europe. *Remote Sens.* 7, 16849-16864.

419 Cammalleri, C., Micale, F., Vogt, J.V., 2015. On the value of combining different modelled soil  
420 moisture products for European drought monitoring. *J. Hydrol.* 525, 547-558.

421 Carlson, T., 2007. An overview of the “Triangle Method” for estimating surface evapotranspiration and  
422 soil moisture from satellite imagery. *Sensors* 7(8), 1612-1629.

423 Crow, W.T., Kumar, S.V., Bolten, J.D., 2012. On the utility of land surface models for agricultural  
424 drought monitoring. *Hydrol. Earth Syst. Sci.* 16, 3451-3460.

425 Dai, A., 2011. Drought under global warming: A review. *Wiley Interdiscip. Rev. Clim. Change* 2, 45-  
426 65.

427 Das, K., Paul, P.K., 2015. Present status of soil moisture estimation by microwave remote sensing.  
428 *Cogent Geoscience* 1, 1084669.



- 429 de Roo, A., Wesseling, C., van Deusen, W., 2000. Physically based river basin modelling within a GIS:  
430 The LISFLOOD model. *Hydrol. Process.* 14, 1981-1992.
- 431 Dirmeyer, P.A., Gao, X., Zhao, M., Guo, Z., Oki, T., Hanasaki, N., 2006. GSWP-2: multimodel analysis  
432 and implications for our perception of the land surface. *Bull. Amer. Meteor. Soc.* 87, 1381–1397.
- 433 Dorigo, W.A., Scipal, K., Parinussa, R.M., Liu, Y.Y., Wagner, W., de Jeu, R.A.M., Naeimi, V., 2010.  
434 Error characterisation of global active and passive microwave soil moisture datasets. *Hydrol.*  
435 *Earth Syst. Sci.* 14, 2605-2616.
- 436 Dorigo, W.A., Chung, D., Gruber, A., Hahn, S., Mistelbauer, T., Parinussa, R.M., Paulik, C., Reimer,  
437 C., van der Schalie, R., de Jeu, R.A.M., Wagner, W., 2016. Soil moisture [in “State of the Climate  
438 in 2015”]. *Bull. Amer. Meteor. Soc.*, 97(8), S31-S32.
- 439 Draper, C., Reichle, R., de Jeu, R., Naeimi, V., Parinussa, R., Wagner, W., 2013. Estimating root mean  
440 square errors in remotely sensed soil moisture over continental scale domains. *Remote Sens.*  
441 *Environ.* 137, 288-298.
- 442 Gruber, A., Su, C.-H., Zwieback, S., Crow, W., Dorigo, W., Wagner, W., 2016. Recent advances in  
443 (soil moisture) triple collocation analysis. *Int. J. Appl. Earth Obs. Geoinf.* 45, 200-211.
- 444 Hain, C.R., Crow, W.T., Mecikalski, J.R., Anderson, M.C., Holmes, T., 2011. An intercomparison of  
445 available soil moisture estimates from thermal infrared and passive microwave remote sensing  
446 and land surface modeling. *J. Geophys. Res.* 116, D15107.
- 447 Hengl, T., de Jesus, J.M., MacMillan, R.A., Batjes, N.H., Heuvelink, G.B.M., Ribeiro, E., et al., 2014.  
448 SoilGrids1km — Global Soil Information Based on Automated Mapping. *PLoS ONE* 9(8),  
449 e105992.



- 450 Houborg, R., Rodell, M., Li, B., Reichle, R., Zaitchik, B., 2012. Drought indicators based on model  
451 assimilated GRACE terrestrial water storage observations. *Wat. Resour. Res.* 48, W07525.  
452 doi:10.1029/2011WR011291.
- 453 Jackson, T.J., 2006. Estimation of Surface Soil Moisture Using Microwave Sensors. *Encyclopedia of*  
454 *Hydrological Sciences, Part 5: Remote Sensing.* doi: 10.1002/0470848944.hsa060.
- 455 Lehner, B., Verdin, K., Jarvis, A., 2008. New global hydrography derived from spaceborne elevation  
456 data, *Eos* 89(10), 93–94.
- 457 Liu, Y.Y., Dorigo, W.A., Parinussa, R.M., de Jeu, R.A.M., Wagner, W., McCabe, M.F., Evans, J.P., van  
458 Dijk, A.I.J.M., 2012. Trend-preserving blending of passive and active microwave soil moisture  
459 retrievals. *Remote Sens. Environ.* 123, 280-297.
- 460 Loew, A., Stacke, T., Dorigo, W., de Jeu, R., Hagemann, S., 2013. Potential and limitations of  
461 multidecadal satellite soil moisture observations for selected climate model evaluation studies.  
462 *Hydrol. Earth Syst. Sci.* 17, 3523-3542.
- 463 McColl, K.A., Vogelzang, J., Konings, A.G., Entekhabi, D., Piles, M., Stoffelen, A., 2014. Extended  
464 triple collocation: Estimating errors and correlation coefficients with respect to an unknown  
465 target. *Geophys. Res. Lett.* 41, 6229-6236.
- 466 Miralles, D.G., Crow, W.T., Cosh, M.H., 2010. Estimating spatial sampling errors in coarse-scale soil  
467 moisture estimates derived from point-scale observations. *J. Hydrometeorol.* 11, 1423-1429.
- 468 Mo, K.C., Long, L.N., Xia, Y., Yang, S.K., Schemm, J.E., Ek, M.B., 2010. Drought indices based on  
469 the Climate Forecast System Reanalysis and ensemble NLDAS. *J. Hydrometeorol.* 12, 185-210.



- 470 Park, J.-Y., Ahn, S.-R., Hwang, S.-J., Jang, C.-H., Park, G.-A., Kim, S.-J., 2014. Paddy Water Environ.  
471 12(1), 77-88.
- 472 Paulik, C., Dorigo, W., Wagner, W., Kidd, R., 2014. Validation of the ASCAT Soil Water Index using  
473 in situ data from the International Soil Moisture Network. *Int. J. Appl. Earth Obs. Geoinfo.* 30, 1-  
474 8.
- 475 Pierdicca, N., Fascetti, F., Pulvirenti, L., Crapolicchio, R., Munõz-Sabater, J., 2015. Analysis of  
476 ASCAT, SMOS, in-situ and land model soil moisture as a regionalized variable over Europe and  
477 North Africa. *Remote Sens. Environ.* 170, 280-289.
- 478 Price, J.C., 1980. The potential of remotely sensed thermal infrared data to infer surface soil moisture  
479 and evaporation. *Water Resour. Res.* 16(4), 787-795.
- 480 Sheffield, J., Goteti, G., Wen, F., Wood, E.F., 2004. A simulated soil moisture based drought analysis  
481 for the United States. *J. Geophys. Res.* 109, D24108. doi:10.1029/2004JD005182.
- 482 Stoffelen, A., 1998. Toward the true near-surface wind speed: Error modelling and calibration using  
483 triple collocation. *J. Geophys. Res.* 103, 7755-7766.
- 484 Srivastava, P.K., Islam, T., Singh, S.K., Gupta, M., Petropoulos, G.P., Gupta, D.K., Wan Jaafar, W.Z.,  
485 Prasad, R., 2016. Soil moisture deficit estimation through SMOS soil moisture and MODIS land  
486 surface temperature. In: *Satellite Soil Moisture Retrieval: Techniques and Applications*, P.K.  
487 Srivastava, G.P. Petropoulos, Y.H. Kerr (Eds.), Elsevier B.V.
- 488 Su, C.-H., Ryu, D., Crow, W.T., Western, A.W., 2014. Beyond triple collocation: Applications to soil  
489 moisture monitoring. *J. Geophys. Res. Atmos.* 119, 6419-6439.





- 490 Verstraeten, W.W., Veroustraete, F., van der Sande, C.J., Grootaers, I., Feyen, J., 2006. Soil moisture  
491 retrieval using thermal inertia, determined with visible and thermal spaceborne data, validated for  
492 European forests. *Remote Sens. Environ.* 101(3), 299-314.
- 493 Wan, Z., Zhang, Y., Zhang, Q., Li, Z.-L., 2002. Validation of the land-surface temperature products  
494 retrieved from Terra Moderate Resolution Imaging Spectroradiometer data. *Remote Sens.*  
495 *Environ.* 83, 163-180.
- 496 Wan, Z., Li, Z.-L., 1997. A physics-based algorithm for retrieving land-surface emissivity and  
497 temperature from EOS/MODIS data. *IEEE Trans. Geosci. Remote Sens.* 35, 980-996.
- 498 Wan, Z., Dozier, J., 1996. A generalized split-window algorithm for retrieving land surface temperature  
499 from space. *IEEE Trans. Geosci. Remote Sens.* 34, 892-905.
- 500 Wilhite, D.A., 2000. Drought as a natural hazard: Concepts and definitions. N: Disasters series.  
501 Routledge Publishers, UK, 213-230.
- 502 World Meteorological Organization, 1986. Intercomparison of models of snowmelt runoff. Operational  
503 Hydrological Report, 23.
- 504 Yilmaz, M.T., Crow, W.T., 2014. Evaluation of assumptions in soil moisture triple collocation analysis.  
505 *J. Hydrometeorol.* 15, 1293-1302.



506 **Tables**

507

508 **Table 1.** Summary of the Pearson correlation coefficient values (average  $\pm$  standard deviation) observed  
 509 for all the regions.

Comparison	ALL	NA	EU	SA	IN	AU
LIS vs. LST	$0.44 \pm 0.09$	$0.41 \pm 0.08$	$0.39 \pm 0.07$	$0.48 \pm 0.09$	$0.44 \pm 0.07$	$0.50 \pm 0.10$
LIS vs. CCI	$0.49 \pm 0.10$	$0.47 \pm 0.09$	$0.42 \pm 0.08$	$0.48 \pm 0.10$	$0.48 \pm 0.08$	$0.58 \pm 0.11$
CCI vs. LST	$0.56 \pm 0.13$	$0.49 \pm 0.14$	$0.37 \pm 0.09$	$0.63 \pm 0.09$	$0.52 \pm 0.10$	$0.68 \pm 0.07$

510

511

512 **Table 2.** Summary of the TC error variance analysis, reporting the spatial average ( $\pm$  standard  
 513 deviation) values observed over each macro-region.

Model	ALL	NA	EU	SA	IN	AU
LIS	$0.48 \pm 0.13$	$0.42 \pm 0.14$	$0.44 \pm 0.12$	$0.54 \pm 0.11$	$0.49 \pm 0.10$	$0.54 \pm 0.14$
LST	$0.44 \pm 0.13$	$0.46 \pm 0.15$	$0.56 \pm 0.10$	$0.37 \pm 0.10$	$0.48 \pm 0.09$	$0.38 \pm 0.11$
CCI	$0.36 \pm 0.18$	$0.46 \pm 0.16$	$0.54 \pm 0.12$	$0.30 \pm 0.14$	$0.38 \pm 0.16$	$0.17 \pm 0.10$

514

515

516 **Table 3.** Fraction of each macro-area (as percentage) where one model outperforms the other two.

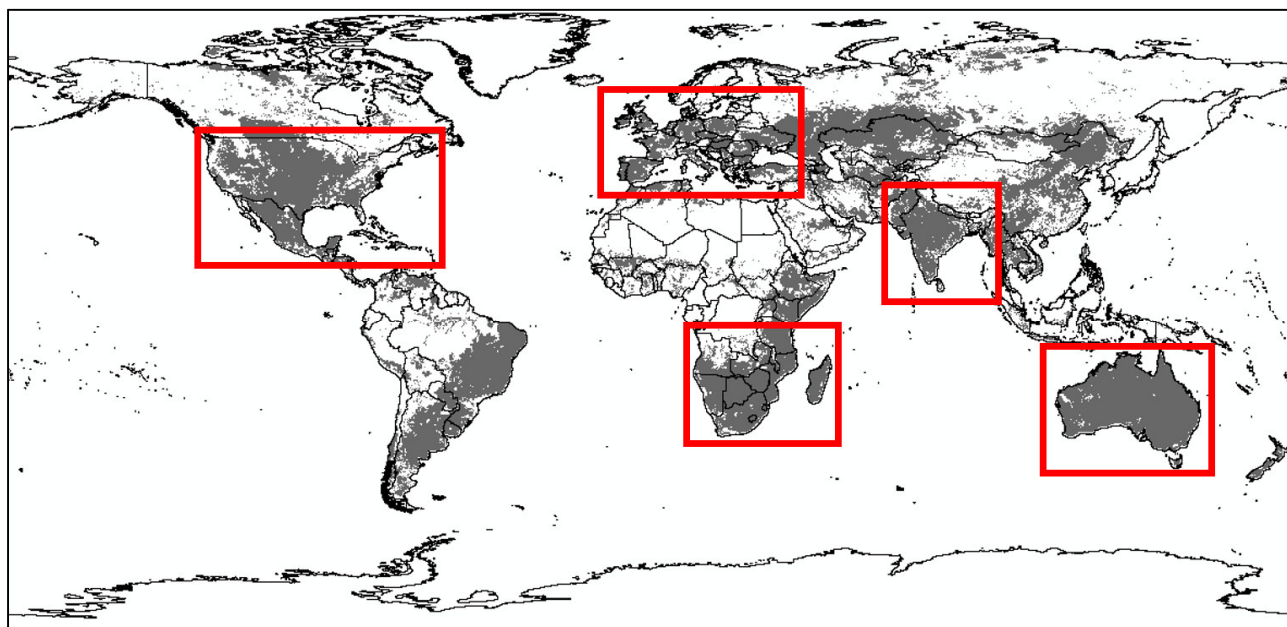
Model	ALL	NA	EU	SA	IN	AU
LIS	25.5	39.2	50.0	10.6	28.2	4.3
LST	25.7	28.8	23.1	36.0	20.3	18.6
CCI	48.8	32.0	26.9	53.4	51.5	77.1

517



518 **Figures**

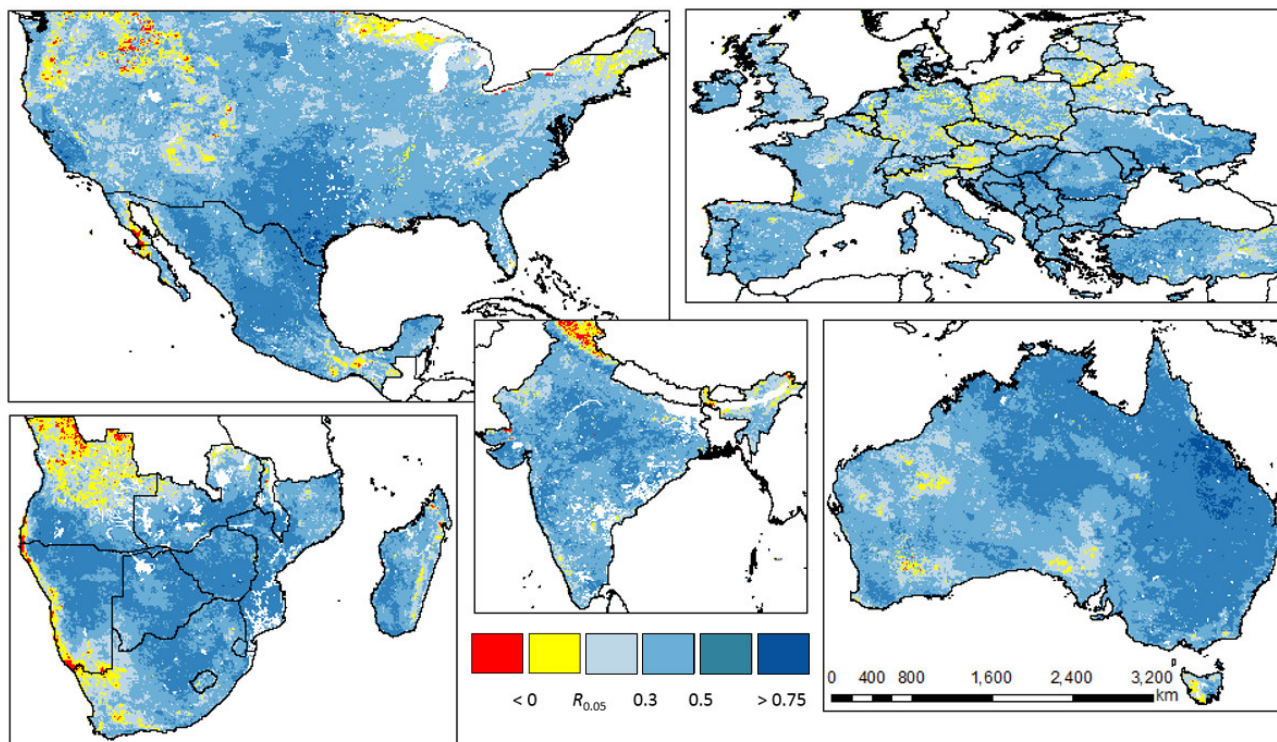
519



520

521 **Fig. 1.** Map of the areas where all the three models are positively significantly linearly correlated (cells  
522 in grey) according to the t-student test at  $p = 0.05$ . The boxes delimitate the macro-regions selected for  
523 the successive analyses.

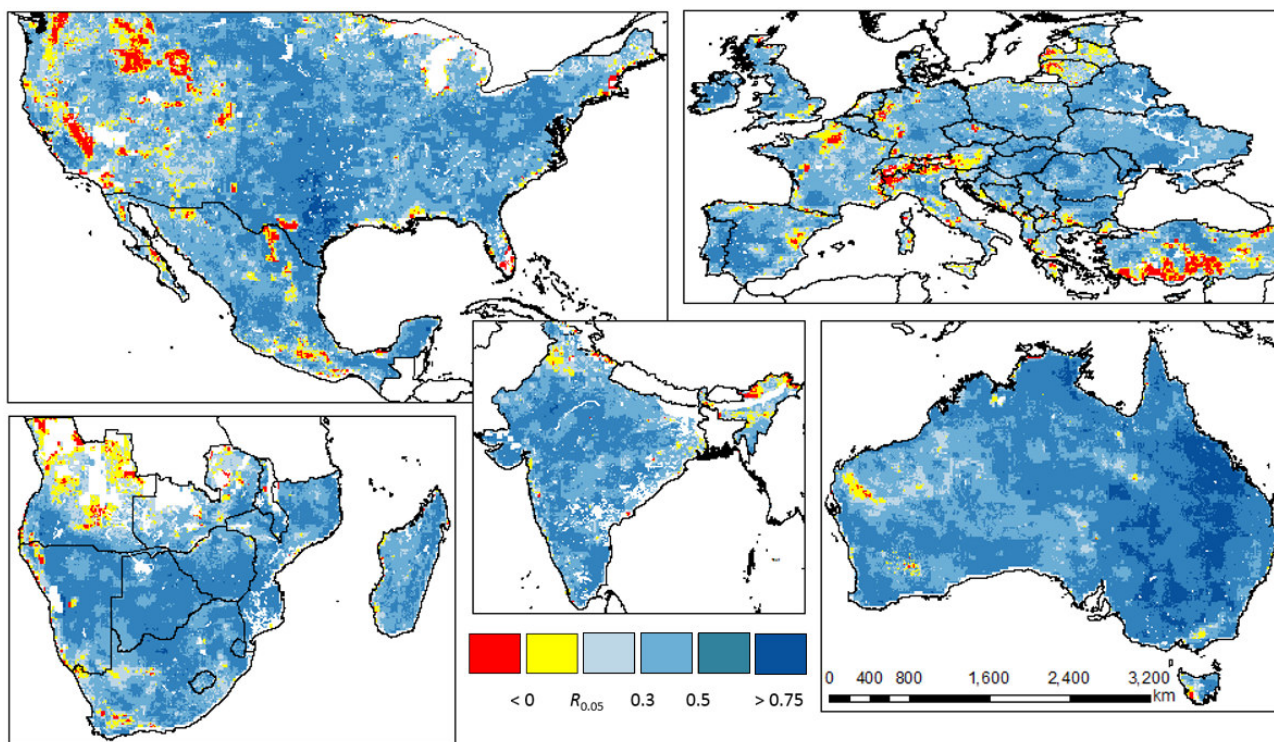
524



525

526 **Fig. 2.** Spatial distribution of the Pearson correlation coefficient ( $R$ ) between Lisflood soil moisture  
527 anomalies (LIS) and land surface temperature anomalies (LST) over the five selected macro-regions.  
528 Values in red and yellow are negatively correlated or not significant at  $p = 0.05$ , respectively.

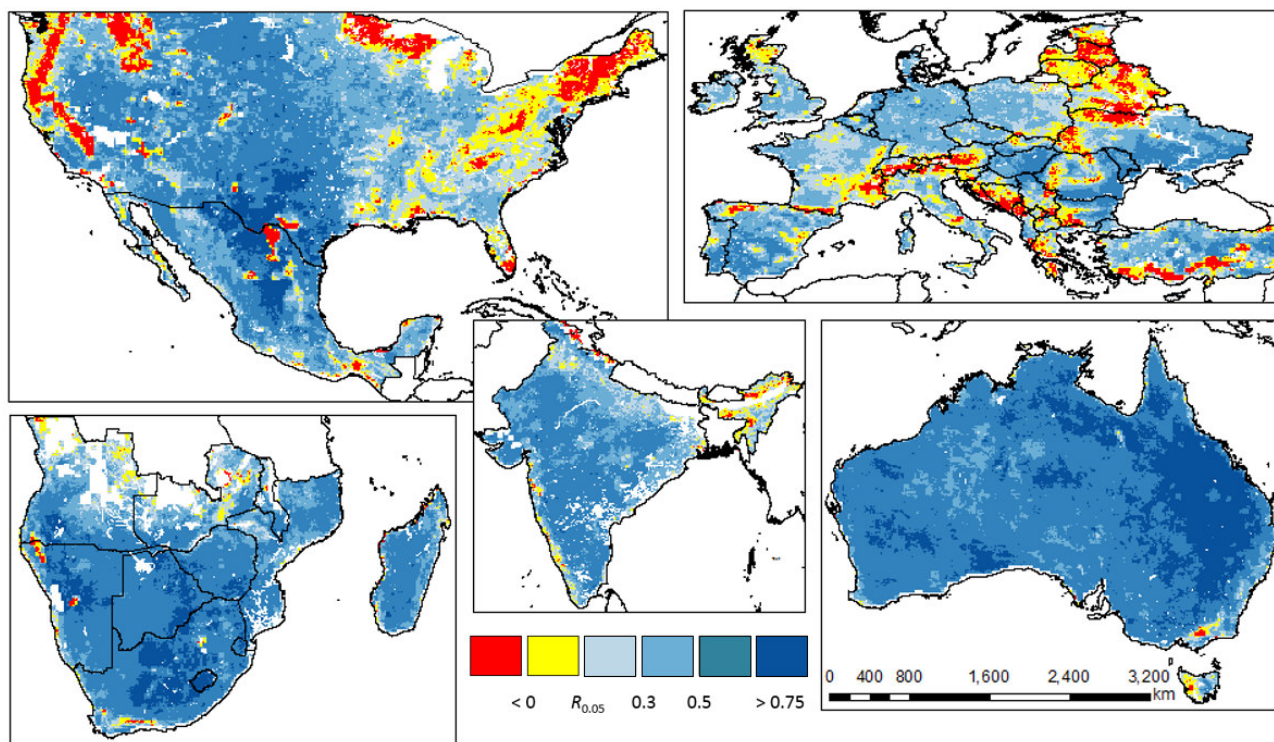
529



530

531 **Fig. 3.** Spatial distribution of the Pearson correlation coefficient ( $R$ ) between Lisflood (LIS) and ESA  
532 Climate Change Initiative (CCI) soil moisture anomalies over the five selected macro-regions. Values in  
533 red and yellow are negatively correlated or not significant at  $p = 0.05$ , respectively.

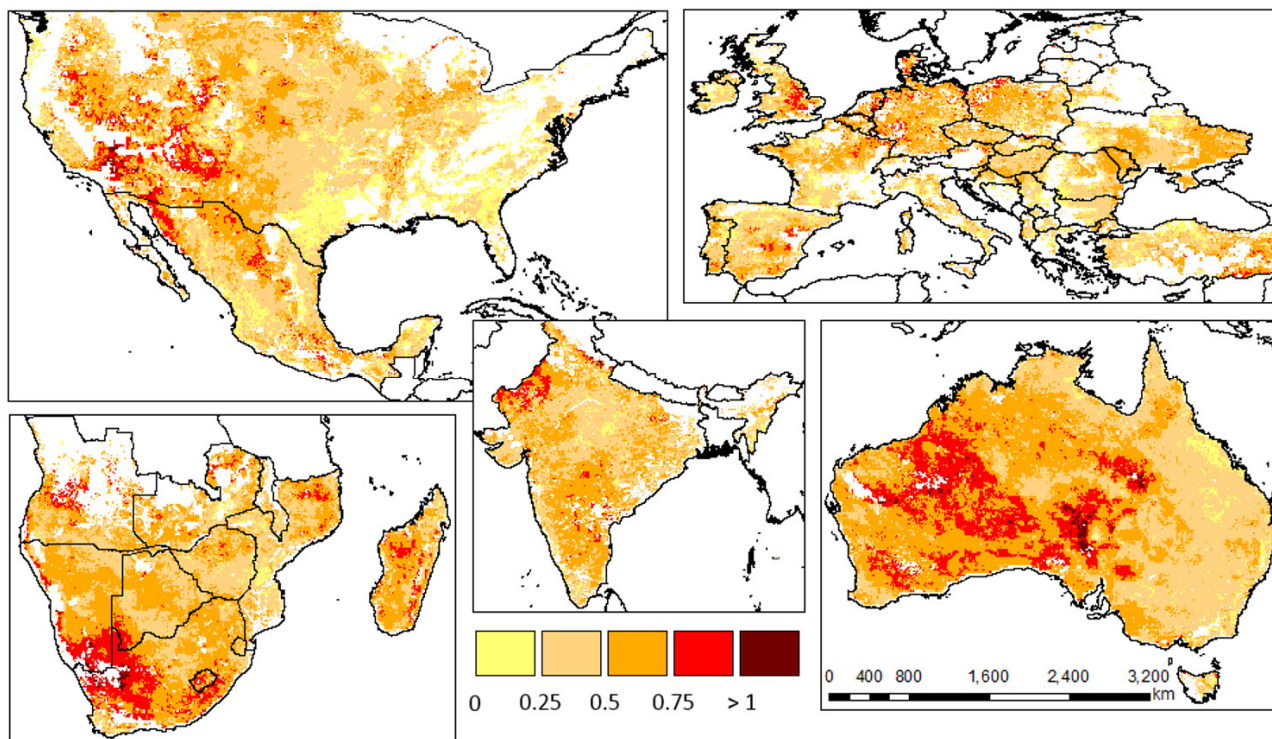
534



535

536 **Fig. 4.** Spatial distribution of the Pearson correlation coefficient ( $R$ ) between ESA Climate Change  
537 Initiative soil moisture anomalies (CCI) and land surface temperature anomalies (LST) over the five  
538 selected macro-regions. Values in red and yellow are negatively correlated or not significant at  $p = 0.05$ ,  
539 respectively.

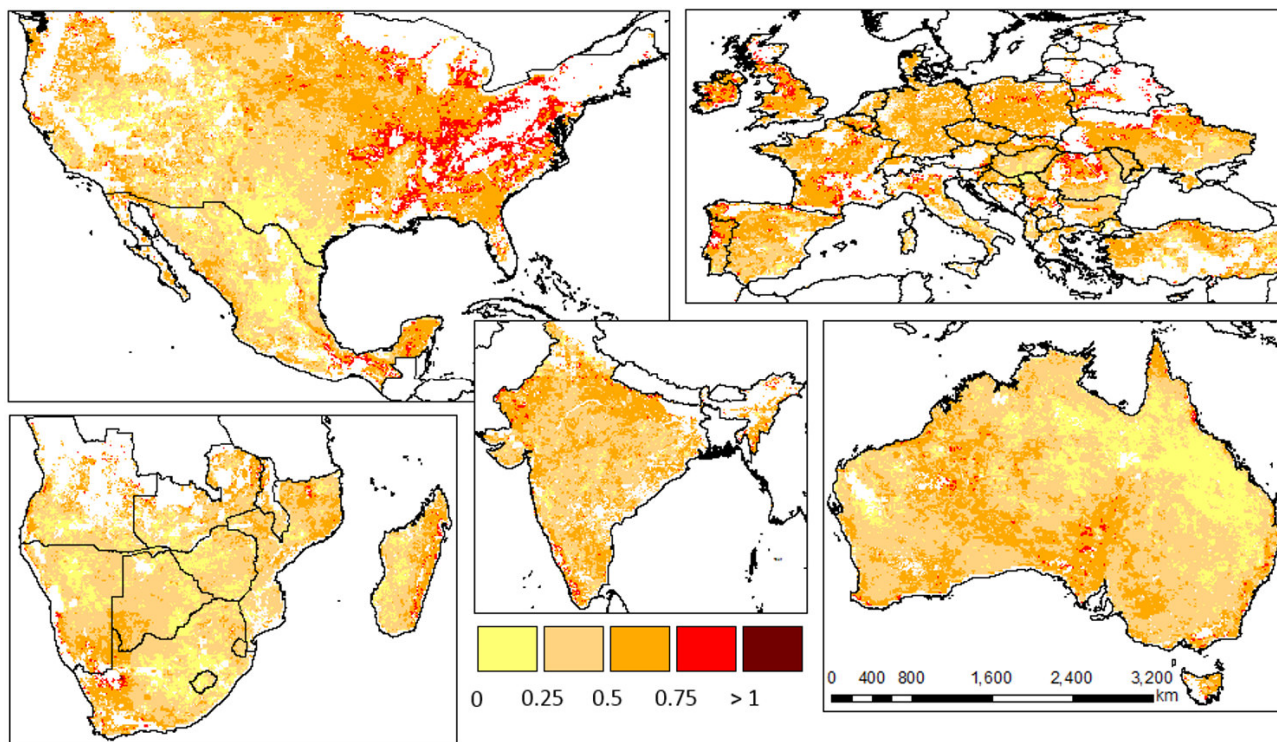
540



541

542 **Fig. 5.** Spatial distribution of the error variance for the Lisflood (LIS) dataset over the five selected  
543 macro-regions.

544

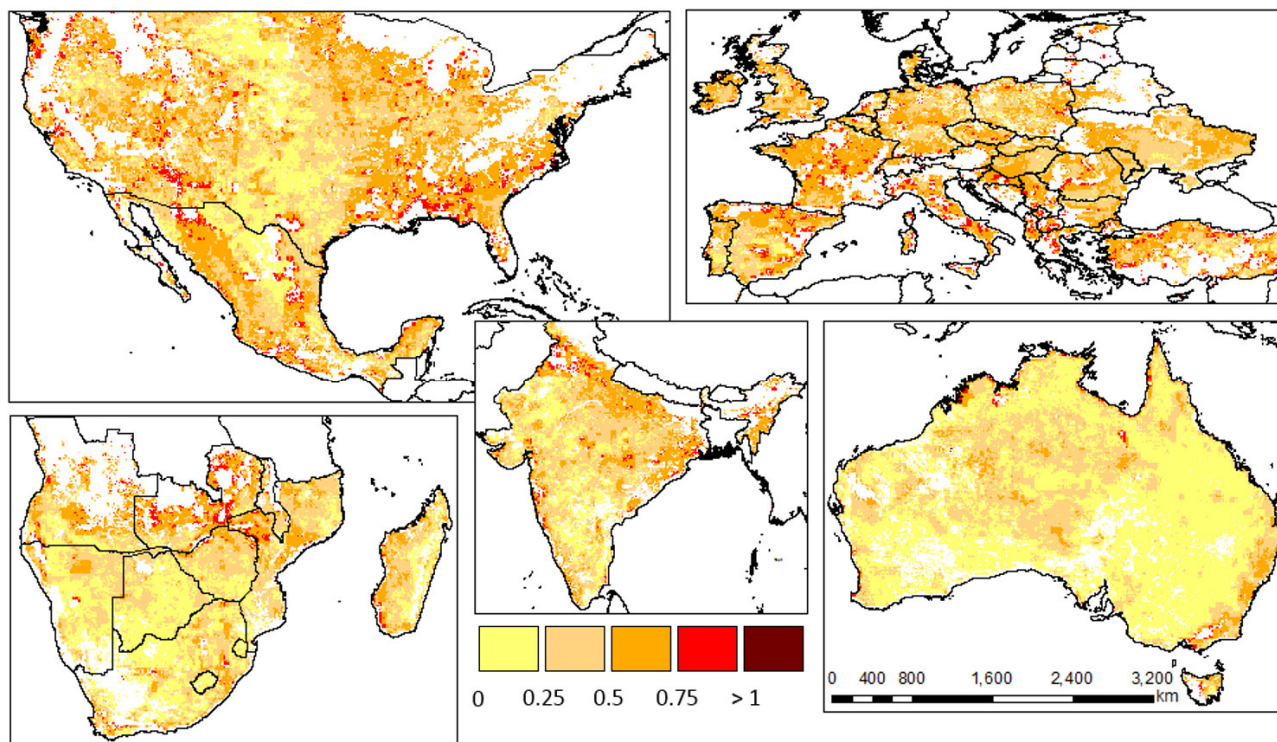


545

546 **Fig. 6.** Spatial distribution of the error variance for the land surface temperature (LST) dataset over the  
547 five selected macro-regions.

548

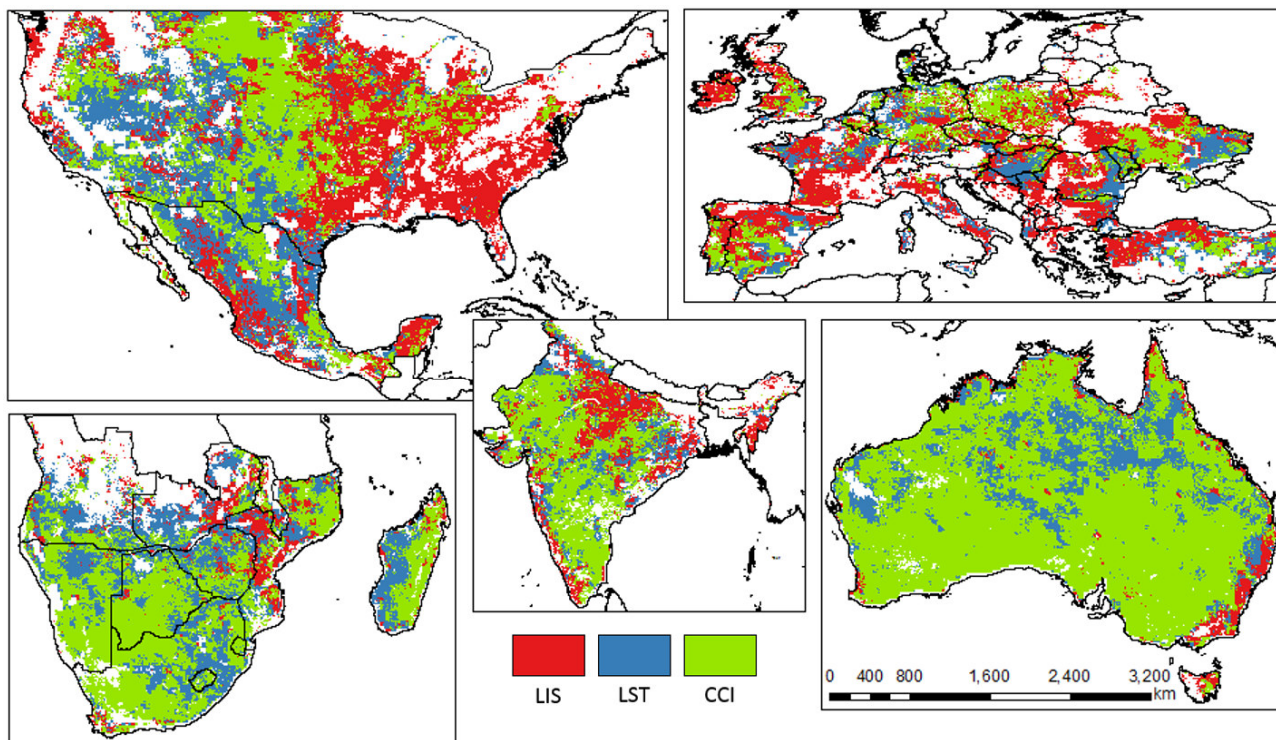




549

550 **Fig. 7.** Spatial distribution of the error variance for the ESA Climate Change Initiative (CCI) dataset  
551 over the five selected macro-regions.

552



553

554 **Fig. 8.** Maps representing the best performing (lowest error variance) dataset for each cell according to  
555 the TC analysis.

556